

Article

Interventions to the Spontaneous Fabrication of Hierarchical ZSM-5 Zeolites by Fluorination-Alkaline Treatment

Zifeng Guo¹, Meihua Hong¹, Yonghua Yu^{2,3}, Guanfeng Liu^{1,*}, Jiazong Zang^{1,*}, Dazhi Zhang², Huimin Gong², Keyu Yang^{2,3} and Shengjun Huang^{2,*}

¹ CenerTech Tianjin Chemical Research and Design Institute Co., Ltd., Tianjin 300131, China

² Division of Fossil Energy Conversion, Dalian Institute of Chemical Physics, Chinese Academy of Sciences, Dalian 116023, China

³ University of Chinese Academy of Sciences, Beijing 100049, China

* Correspondence: liugf7@cnooc.com.cn (G.L.); zangjzh2@cnooc.com.cn (J.Z.); huangsj@dicp.ac.cn (S.H.)

Abstract: The sequential fluorination-alkaline treatment protocol has been applied for the tailoring of siliceous ZSM-5 zeolite. The original spontaneous growth of mesoporosity in alkaline medium is altered due to the antecedent fluorination step. The outcome is demonstrated by the apparent delay in the mesoporosity growth, whose essential duration for the well-defined mesoporosity is therefore extended from 30 min to 60 min. A low fluorination level decelerates the mesoporosity growth, whereas a high fluorination level enables the achievement of the mesoporosity. These impacts are closely linked with the alteration to the states of Al sites as the function of fluorination level. Compared to the states of Al sites in the pristine and steamed zeolites, the electronic and steric consequences on the environment of Al species by fluorination is proposed for the interplay with the alkaline medium for the mesoporosity growth.



Citation: Guo, Z.; Hong, M.; Yu, Y.; Liu, G.; Zang, J.; Zhang, D.; Gong, H.; Yang, K.; Huang, S. Interventions to the Spontaneous Fabrication of Hierarchical ZSM-5 Zeolites by Fluorination-Alkaline Treatment. *Catalysts* **2022**, *12*, 954. <https://doi.org/10.3390/catal12090954>

Academic Editors: Maja Milojević-Rakić and Danica Bajuk-Bogdanović

Received: 30 June 2022

Accepted: 17 August 2022

Published: 28 August 2022

Publisher's Note: MDPI stays neutral with regard to jurisdictional claims in published maps and institutional affiliations.



Copyright: © 2022 by the authors. Licensee MDPI, Basel, Switzerland. This article is an open access article distributed under the terms and conditions of the Creative Commons Attribution (CC BY) license (<https://creativecommons.org/licenses/by/4.0/>).

Keywords: hierarchical zeolites; fluorination; siliceous ZSM-5; dealumination

1. Introduction

Zeolites are crystalline materials with well-defined microporosity, good hydrothermal stability, tunable compositions and functionalities. These features not only lead to their feasible applications in various industrial petrochemical processes including catalytic cracking, alkylation, aromatization, etc., but also render promising prospects in the productions of fine chemicals [1–4]. Stringent situation of feedstocks compositions for petrochemical processes and appearing versatile “platform” compounds from biomass resource bring forth more requirements for the zeolite-based catalysts: enhanced mass transfer efficiency, higher utilization efficiency of active sites and better resistance to deactivation [2,5]. Nevertheless, the pure micropore networks (<1.2 nm) of microporous zeolites may constrain their performances in these emerging fields [6,7]. Hierarchical zeolites, with the intrinsic micropore and a coupled intra/intercrystalline mesopore networks, have proved their potential in the emerging processes including synthesis of bulky fine chemicals, methanol conversions, pyrolysis and biomass conversions [8–12]. Therefore, synthesis of hierarchical zeolites attracts extensive attentions from basic research and industrial community [13–18].

Alkaline treatment has been proved as a cost-efficient top-down methodology for the construction of hierarchical porosity in various industrial-relevant zeolites with versatile topologies (MFI [19,20], FAU [21], MOR [22,23], BEA [24,25], etc.), which demands a precondition of optimal Si/Al range with 25–50. The underlying process for the achievement of the hierarchical porosities roots from a dynamic equilibrium between dissolution of matrix and reverse surface passivation in alkaline medium, which is regulated by the environments and transformation of Al sites inside zeolite [20,26]. However, in the case of microporous zeolites with starting optimal Si/Al ratios, the fabrication of hierarchical porosity has been displayed as a spontaneous process under the suitable treatment conditions. In other

words, the fabrication of hierarchical porosities is confined to the limited alterations by the external parameters including temperature and concentration of alkaline solution [27]. The protocols beyond the external parameters are desirable given the resulting flexibility in porosity tailoring.

In this work, a fluorination-alkaline sequential treatment methodology is applied to the tailoring of MFI zeolite with optimal Si/Al ratio (Si/Al = 34). Accordingly, the initial spontaneous construction of hierarchical porosities is artificially intervened, which results in significant alterations to the achievement of hierarchical porosities. Compared to the usual alkaline treatment, the construction of hierarchical porosities is apparently delayed by the antecedent fluorination step. The resulting porosities still can be tailored and display the dependence on the antecedent fluorination step as the function of fluorination level. The implication of the antecedent fluorination step in the sequential alkaline treatment is proposed as the intervention to the electronic and steric of Al species, upon which their interplay with the alkaline medium is altered for the mesoporosity growth. Our results display the feasibility of beyond the spontaneous construction of hierarchical porosity upon alkaline treatment and therefore enrich the associated mechanistic understandings on the governing interplays for the mesoporosity growth.

2. Results and Discussion

The fluorination-desilication significantly alters the porosity development in the siliceous ZSM-5 zeolite. In line with the reported results, the spontaneous alkaline treatment conditions give rise to a combined type-I and type-IV with a hysteresis in the isotherm of AT(65,30)-Z5, which corresponds to a substantial contribution centered around 10 nm in the pore size distribution (PSD) curves. In contrast, mesoporosity developments in fluorinated Z5 samples are barely observed upon the alkaline treatment at 65 °C for 30 min. As shown in Figures 1 and 2, the isotherms of AT(65,30)-FZ5a and AT(65,30)-FZ5b only display subtle hysteresis loops, and the derived PSD curves evidence the suppressed contributions compared to that of AT(65,30)-Z5. Nevertheless, significant mesoporosities appear again upon longer treatment duration of 60 min. As shown in Figures 1 and 2, pronounced hysteresis loops are observed in the isotherms of AT(65,60)-FZ5a and AT(65,60)-FZ5b, corresponding to significant contributions in the derived PSD curves. The preceding fluorination level has substantial impacts on the final mesoporosity. The mesopore contribution of AT(65,60)-FZ5a shifts to a smaller dimension around 7 nm, whereas the PSD curve of AT(65,60)-FZ5b similarly concentrates on the typical dimension for AT(65,30)-Z5 around 10 nm. Apparently, the antecedent fluorination step is responsible for the alterations to mesoporosity development. Analogously, alteration to the mesopore dimension can be also observed for the sample upon a low-level fluorinated precursor (Figure 1b). The textural parameters derived from the N₂ adsorption-desorption isotherms are shown in Table 1. The low-level fluorination step (e.g., 0.12 wt% for FZ5a) dramatically enhances the mesoporosity development in the subsequent alkaline treatment. Accordingly, the mesoporous surface area (S_{meso}) and mesopore volume (V_{meso}) of AT(65,60)-FZ5a achieve 175 m²/g and 0.29 cm³/g, respectively, which are obviously higher than the parameters (S_{meso} 81 m²/g and V_{meso} 0.18 cm³/g) of AT(65,30)-Z5. Compared to the microporosities of pristine Z5 and AT(65,30)-Z5, the micropore surface area (S_{micro} , 362 m²/g and 358 m²/g) and micropore volume (V_{micro} 0.16 cm³/g) decreased by approximately 23% and 25%, respectively, for AT(65,60)-FZ5a. The high-level fluorination step (0.72 wt% F) leads to serious reductions in microporosities (S_{micro} 332 m²/g and V_{micro} 0.15 cm³/g) for AT(65,60)-FZ5b, but brings about less pronounced enhancement in mesoporosities. The SEM and HRTEM images in Figure 3 show that the pristine zeolite has smooth and characteristic morphology. In comparison to the pristine zeolite with smooth surface, dense pore openings throughout the external surface were obtained by fluorination-alkaline treatment, while the cube-shape morphology is still well preserved (Figure 4a–d). The HRTEM images exhibit the alternately bright and dark contrast areas in Figure 5a–d. The light patches are associated with the presence of mesopores in the obtained hierarchical zeolites. Physical adsorption, SEM and

HRTEM observations confirm the intracrystalline nature of the created mesopores by the fluorination-alkaline treatment.

Table 1. Textural properties of pristine and fluorination-alkaline treated ZSM-5 samples.

Sample	Yield [a] [%]	S_{BET} [b] [m^2g^{-1}]	S_{micro} [c] [m^2g^{-1}]	S_{meso} [d] [m^2g^{-1}]	V_{micro} [d] [cm^3g^{-1}]	V_{meso} [e] [cm^3g^{-1}]	V_{pore} [f] [cm^3g^{-1}]
Z5	-	377	362	15	0.16	0.06	0.22
AT(65,30)	65	439	358	81	0.16	0.18	0.34
AT(65,60)-aFZ5	72	452	277	175	0.12	0.29	0.41
AT(65,60)-bFZ5	84	440	332	108	0.15	0.25	0.40
AT(80,30)	42	446	221	225	0.10	0.34	0.44
AT(80,30)-aFZ5	66	475	280	195	0.12	0.35	0.47
AT(80,30)-bFZ5	79	445	324	121	0.15	0.29	0.44

[a] Grams of solid after treatment per gram of starting material. [b] BET method. [c] $S_{\text{BET}}-S_{\text{meso}}$. [d] t -plot method. [e] $V_{\text{pore}}-V_{\text{micro}}$. [f] Volume of N_2 adsorbed at $P/P_0 = 0.99$.

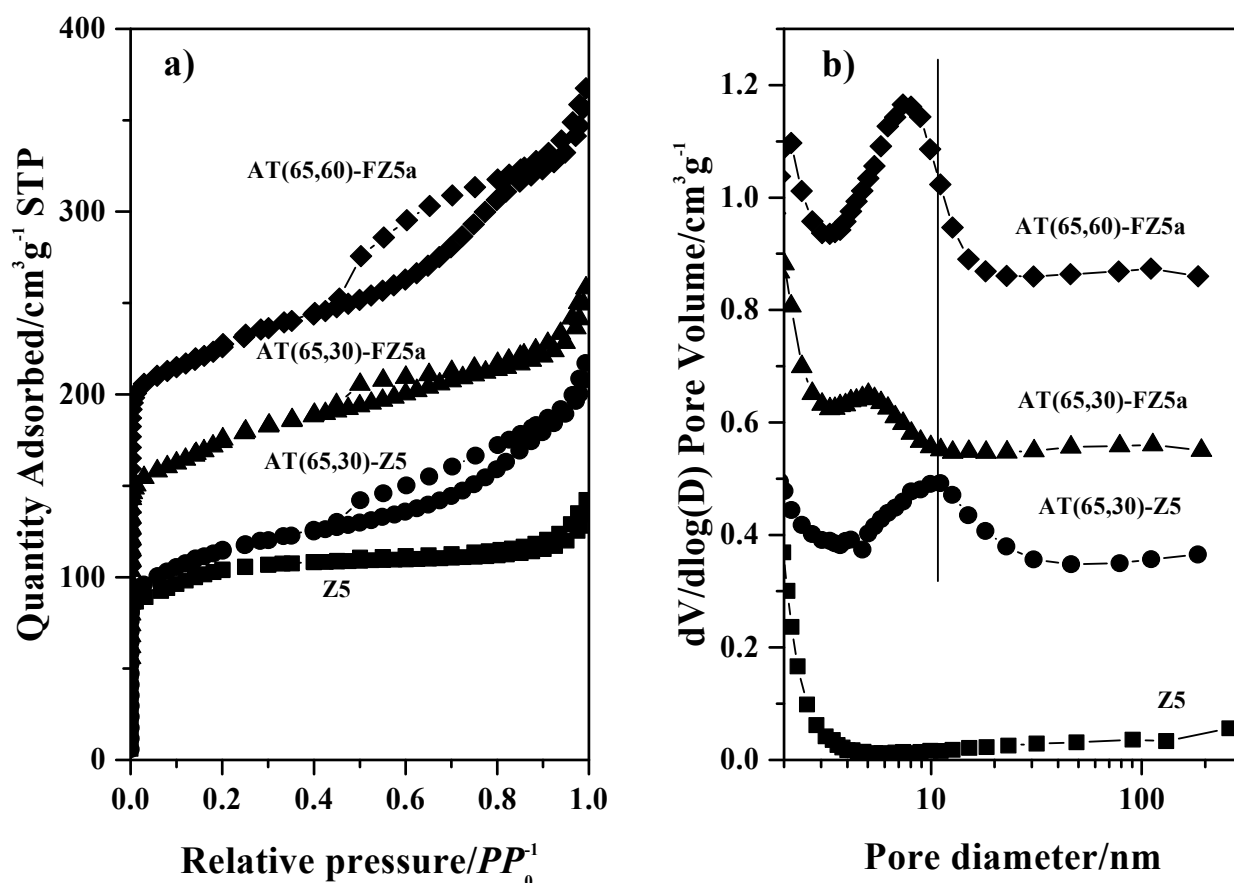


Figure 1. (a) N_2 adsorption-desorption isotherms of treated samples. (b) BJH pore size distribution derived from the adsorption branches of the isotherms. The isotherms for AT(65,30)-FZ5a and AT(65,60)-FZ5a were offset vertically by 50 and 100 cm^3g^{-1} , respectively. (b) Barrett-Joyner-Halenda (BJH) pore size distribution (PSD) data derived from the adsorption branches of the isotherms. The PSD curves of AT(65,30)-Z5, AT(65,30)-FZ5a and AT(65,60)-FZ5a were offset vertically by 0.3, 0.5 and 0.8 cm^3g^{-1} , respectively.

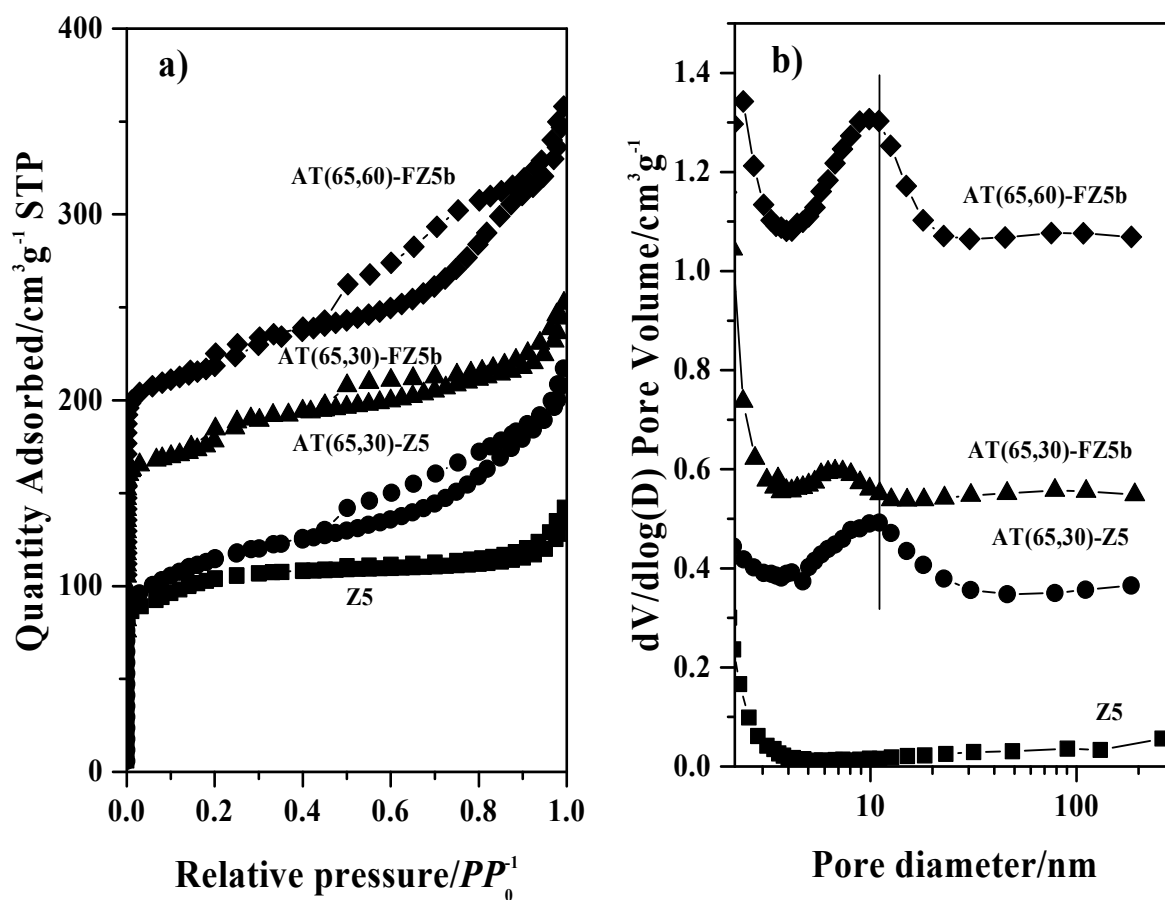


Figure 2. (a) N_2 adsorption-desorption isotherms of treated samples at 65 °C. (b) BJH pore size distribution derived from the adsorption branches of the isotherms. The isotherms for AT(65,30)-FZ5b and AT(65,60)-FZ5b were offset vertically by 70 and 100 $cm^3 g^{-1}$, respectively. (b) Barrett-Joyner-Halenda (BJH) pore size distribution (PSD) data derived from the adsorption branches of the isotherms. The PSD curves of AT(65,30)-Z5, AT(65,30)-FZ5b and AT(65,60)-FZ5b were offset vertically by 0.3, 0.5 and 1.0 $cm^3 g^{-1}$, respectively.

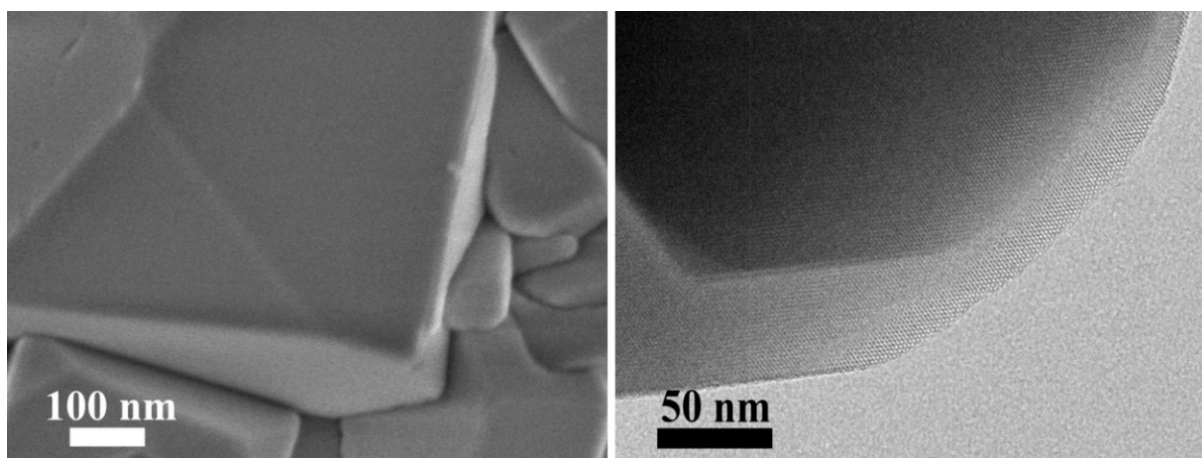


Figure 3. FESEM and HR-TEM micrographs of pristine ZSM-5 zeolite.

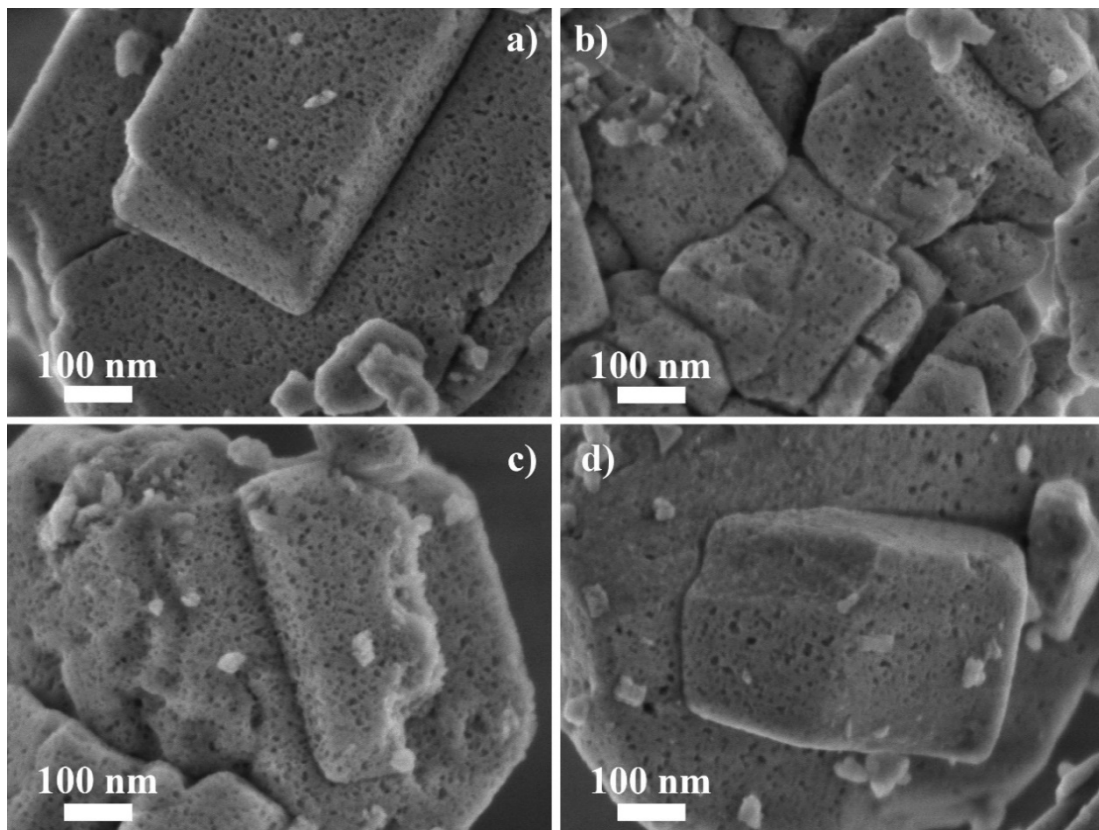


Figure 4. FESEM micrographs of fluorination-alkaline treated samples. (a) AT(65,60)-FZ5a, (b) AT(65,60)-FZ5b, (c) AT(80,30)-FZ5a, (d) AT(80,30)-FZ5b.

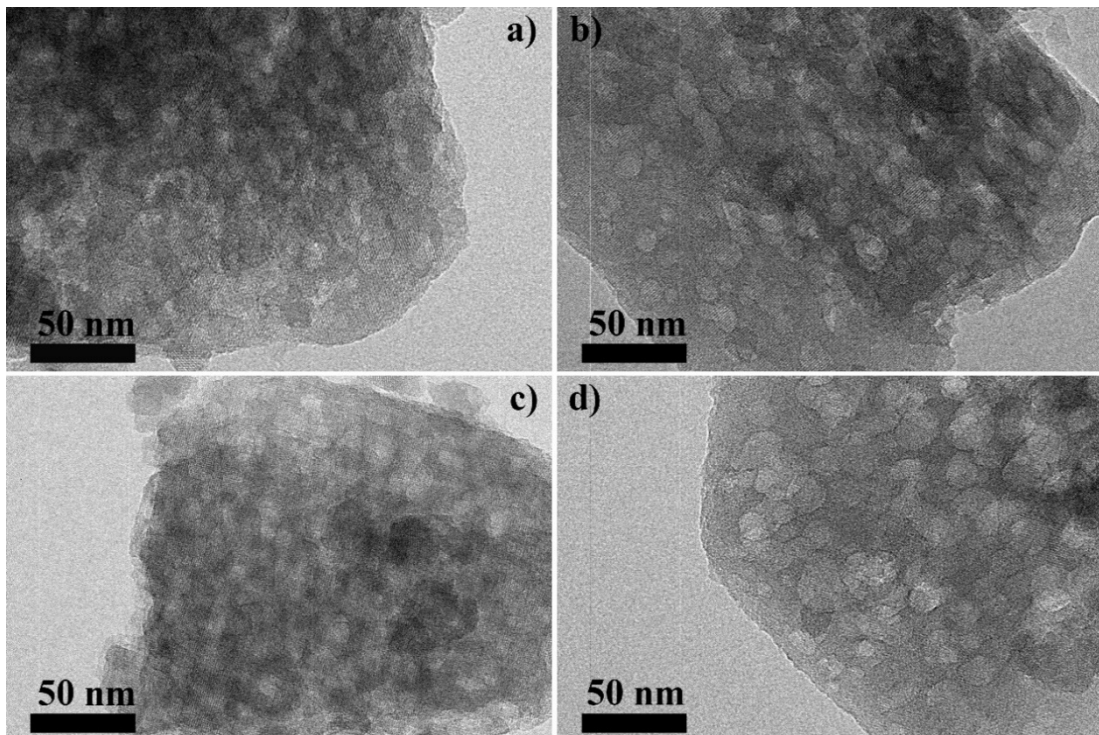


Figure 5. TEM micrographs of fluorination-alkaline treated samples. (a) AT(65,60)-FZ5a, (b) AT(65,60)-FZ5b, (c) AT(80,30)-FZ5a, (d) AT(80,30)-FZ5b.

The impact of fluorination step on the state of Al sites is reflected by the ^{27}Al MAS NMR spectroscopy. As shown in Figure 6, the pristine ZSM-5 exhibits a significant resonance at 55 ppm, which is assigned to the four-coordinated framework Al sites.

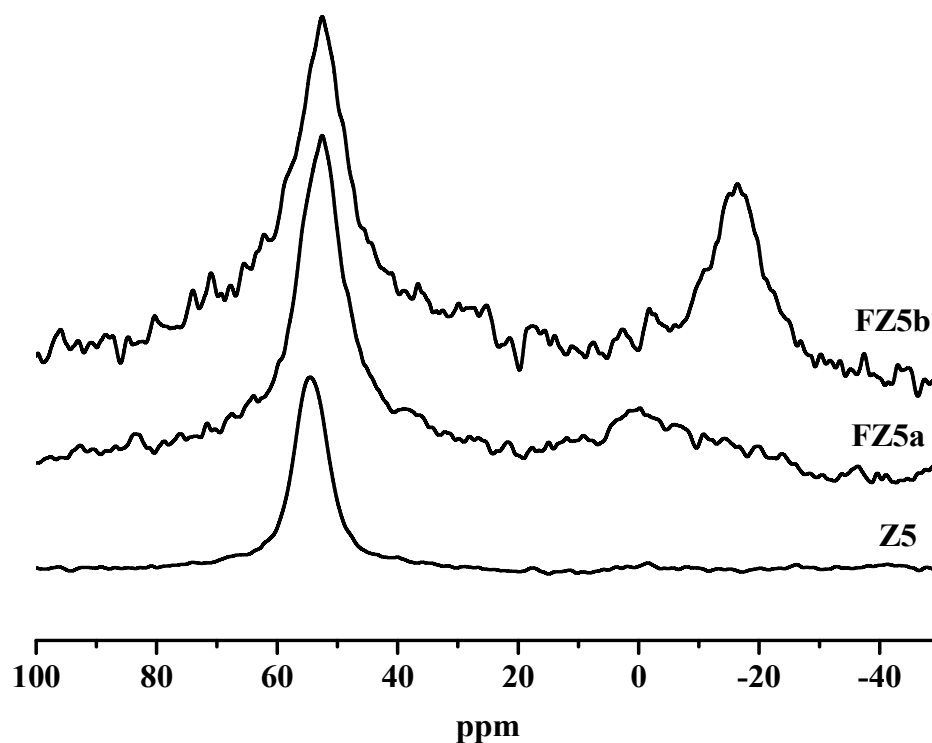


Figure 6. ^{27}Al MAS NMR of pristine ZSM-5 zeolite and fluorinated zeolites.

Upon fluorination treatment, a shift of resonance from 55 ppm to 54 ppm is observed for the fluorinated FZ5a and FZ5b, reflecting the interaction/perturbation of fluoride with the framework Al sites. At low level fluorination, the resonance at 0 ppm appears, indicating the parallel dealumination of framework Al sites to non-framework Al species. However, the high fluorination level leads to the reduction of the resonance at 0 ppm and a significant resonance at -16 ppm, the latter of which is assigned to the AlF_3 phases [28]. Therefore, the fluorination of siliceous ZSM-5 zeolites leads to various alterations to the framework sites as the function of fluorination level: perturbation of the environment of framework Al sites due to the Al-F complexation, dealumination to the octa-coordinated non-framework Al species and formation of the AlF_3 phase. The alterations, in particular the latter two different modes of dislodge of framework Al sites, intervene the sequential development of mesoporosity according to their interplay with the alkaline treatment conditions. Upon the low fluorination level, the generated non-framework Al sites are responsible for poor mesoporosity development in the sequential alkaline treatment at 65°C for 30 min. It is interesting to note that such a decelerating effect is overcome by the extension of alkaline treatment duration to 60 min as reflected by the appearance of significant mesoporosity in the BJH profile of AT(65,60)-FZ5a. The similar delayed mesoporosity growth is also observed for the alkaline treatment of FZ5b along the transformation to the AlF_3 phase at the higher fluorination level, in which the significant mesoporosity is observed until the longer treatment duration of 60 min. It is worthy of noting that the “decelerating effect” or “delayed effect” imposed by fluorination is intrinsically different to the “inhibitive effect” imposed by the usual dealumination of steaming. The antecedent dealumination of steaming of siliceous ZSM-5 zeolites ($\text{Si}/\text{Al} = 34$) has been reported to disable the sequential mesoporosity development by alkaline treatment, which was assigned to the inhibitive effect by the non-framework Al species due to the steaming treatment. Moreover, our comparative steaming-alkaline treatment experiments prove that such inhibitive effects cannot be overcome by the extension of alkaline treatment

duration. The corresponding PSD profile in Figure 7 provides evidence of the absence of mesoporosity development in AT(65,60)-ST-Z5 by sequential steaming-alkaline treatment despite the extended alkaline treatment duration of 60 min.

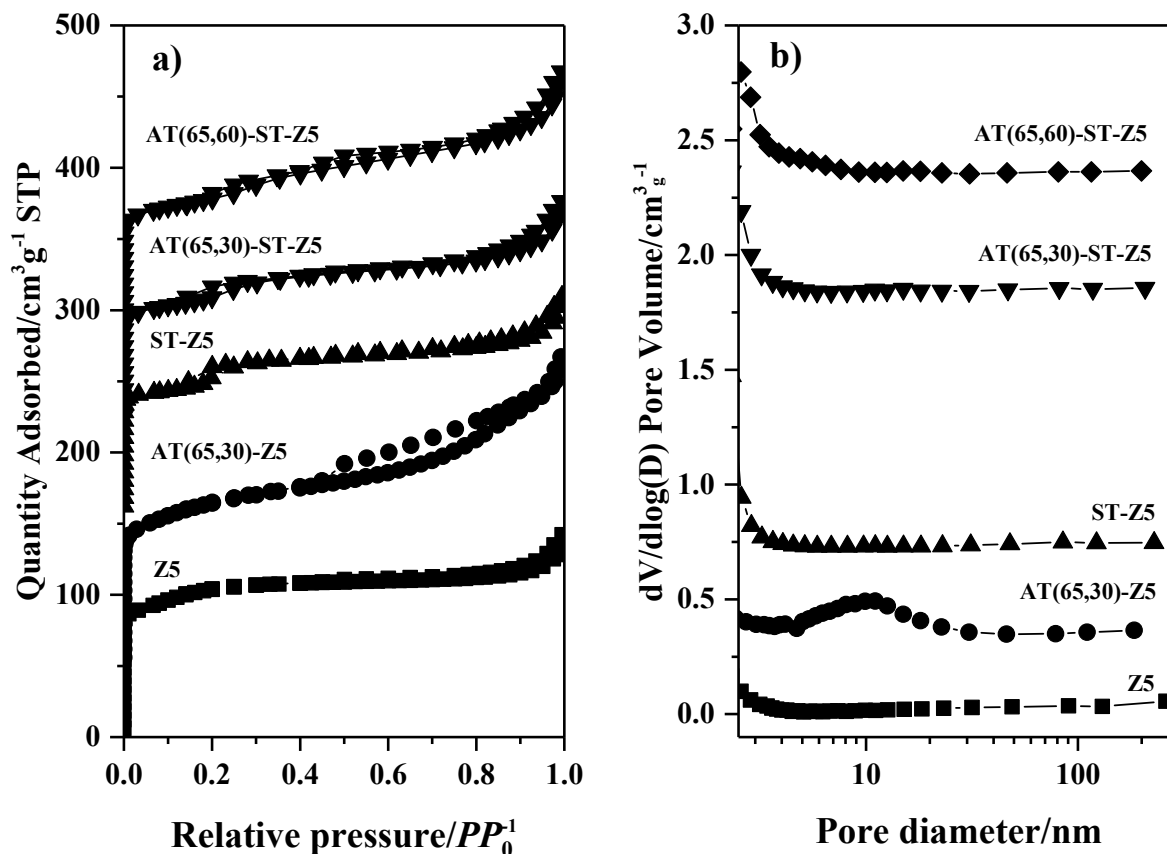


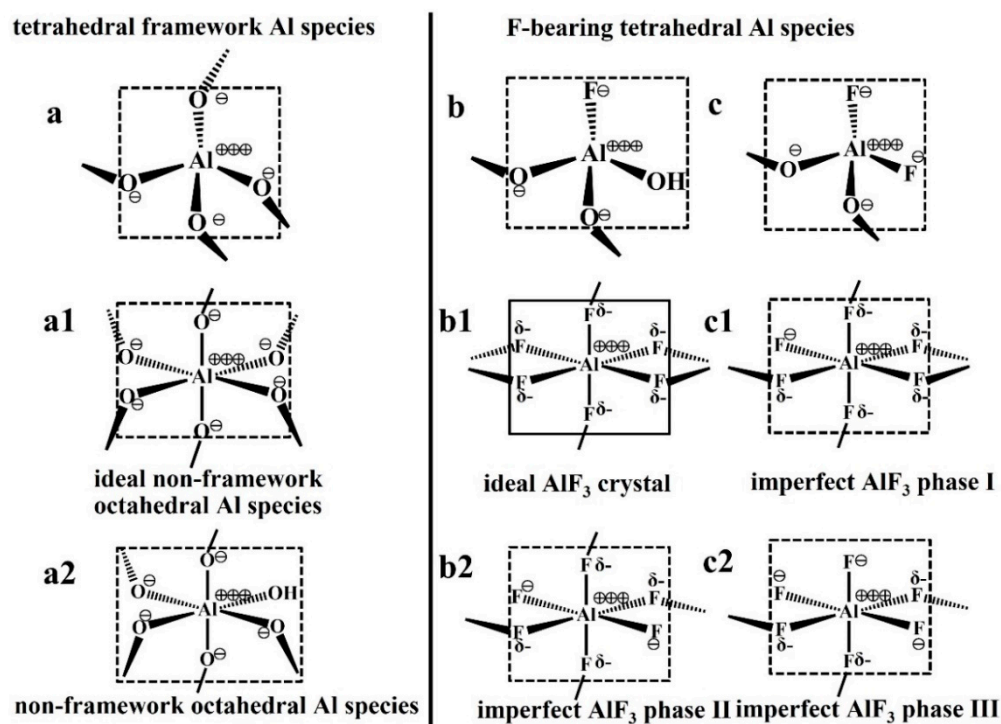
Figure 7. (a) N_2 adsorption-desorption isotherms of steaming-alkaline treated samples. (b) BJH pore size distribution derived from the adsorption branches of the isotherms. The isotherms for AT(65,30)-Z5, ST-Z5, AT(65,30)-ST-Z5 and AT(65,60)-ST-Z5 were offset vertically by 50, 150, 220 and 270 $cm^3 g^{-1}$, respectively. (b) Barrett–Joyner–Halenda (BJH) pore size distribution (PSD) data derived from the adsorption branches of the isotherms. The PSD curves of AT(65,30)-Z5, ST-Z5, AT(65,30)-ST-Z5 and AT(65,60)-ST-Z5 were offset vertically by 0.3, 0.7, 1.8 and 2.3 $cm^3 g^{-1}$, respectively.

Therefore, the above results indicate that the mode of mesoporosity growth can be tailored to an intermediate mode between spontaneous manner and complete inhibitive status. The underlying process of spontaneous manner relies on the framework Al-directing dissolution of microporous zeolite matrix, which is governed by the dynamic transformation of framework Al sites [20]. The apparent outcome of such spontaneous manner is shown as the requirement on an optimal Si/Al ratio range from 25 to 50 for the mesoporosity development [20]. However, the presence of non-framework Al species passivates the mesoporosity development despite their optimal overall Si/Al ratios in this case and other reports [29]. As the intermediate mode, the fluorination step introduces a different response to the alkaline medium, which has close association with the progress of mesoporosity. Based on the ^{27}Al MAS NMR results, the comparison among the non-framework Al species and the fluorinated Al species are depicted in Scheme 1. Upon the mild fluorination level for FZ5a, the perturbation to the $[AlO_4]$ units is proposed to result in the formation of F-bearing tetrahedral Al sites. The high-level fluorination leads to the formation of aluminum fluoride phases including the ideal phases and their imperfect counterparts [28]. Such structural alterations induce a different response to the alkaline medium due to the imposed electronic and steric consequences. The link with the origin of the inhibitive effect

of the non-framework species enlightens the understanding of the decelerating effects by the fluorinated phases. As an ideal structural model, the non-framework Al species is characteristic of the unit with an octahedral coordination [30]. Compared to the tetrahedral framework Al sites (illustration a vs. illustration a1 in Scheme 1), the octahedral non-framework Al unit bears a higher density of negative charge density. From the viewpoint of the charge distribution, the creation of such ideal octahedral units assembles the negative charge, and therefore creates harder bastions to the alkaline ions, which are proposed to account for the inhibitive effect for mesoporosity growth due to the electron repulsive between negative charged Al-bearing species and hydroxides ($[\text{OH}]^-$). Given the electronically neutral character of the overall zeolite, such impacts refer to the redistribution of negative charges within the zeolite framework. At least, the fluorination step introduces the electronic and steric impacts on the framework and non-framework Al species. As shown in Scheme 1, the fluorine ligand enhances the charge density of the tetrahedral unit due to its smaller radius, which inhibits the interplay with hydroxides. On the other hand, the introduction of the fluorine ligand reduces the symmetry of the tetrahedron and therefore enhances the interplay with the alkaline media. In the case of octahedral state, the introduction of fluorine ligand reduces the negative charge's density along with reducing the size of the unit. The balance of these opposite factors decides the overall interplay with the alkaline hydroxides and the corresponding growth of mesoporosity. Upon the low level of fluorination, the enhanced charge effect overtakes that of the reduced symmetry, which therefore decelerates the mesoporosity. As the comparison with pure O-coordinated non-framework Al species upon steaming treatment, the F-coordinated non-framework Al species ease the strong repulsion to the hydroxides, which enables the mesoporosity growth inside the fluorinated zeolites. Compared to the inhibitive effect by the steaming step, the fluorination step brings the enabling impact for the generation of mesoporosity despite its apparent longer essential duration. It is interesting to note that the essential duration can be eliminated by the harsh alkaline treatment conditions. The enhanced alkaline treatment temperature accelerates the mesoporosity development. Upon alkaline treatment at 80 °C, the pronounced hysteresis loops and significant contributions are observed upon the duration of 30 min as shown by the N_2 adsorption-desorption isotherms and the derived PSD curves of AT(80,30)-aFZ5 and AT(80,30)-bFZ5, respectively (Figure 8). Meanwhile, upon the harsh alkaline treatment, the fluorination step fully demonstrates its beneficial impacts on the achievement of significant well-defined mesoporosity. Therefore, this suggests the alteration of the interplay between fluorine-bearing species and alkaline medium as the function of fluorination level and treatment conditions.

The sequential fluorination-alkaline treatment protocol has been successfully designed for the creation of hierarchical porosities inside Al-rich ZSM-5 zeolites ($\text{Si}/\text{Al} < 15$). In the case of the Al-rich ZSM-5 zeolites, the critical roles of fluorination have been owed to the F-Al complexation effects, which are responsible for the alleviation of initial strong resistance of high-density Al sites to the alkaline medium and the regulated hydrolysis process to sustain the growth of mesoporosity. The application of fluorination-alkaline treatment protocol to the siliceous ZSM-5 uncovers a different side of the fluorination step which cannot be observed in the case of Al-rich ZSM-5 counterpart.

The interplays between non-framework Al species and mesoporosity development still demand fundamental insights, which, however, are confronted with multiple and long-term challenges including the elaboration of the precise structure of non-framework Al species and the mechanistic understandings on the working modes [30]. It should be noted that the schematic descriptions in Scheme 1 are simplified ideal models, and their amending to the complexed non-framework Al species requires further efforts. Our attempt is based on our accumulation on this topic for years, and is beneficial to stimulate more discussion and insights [23,28,31].



Scheme 1. The Schematic depiction of the comparison among the non-framework Al species (a) and the fluorinated Al species (b,c). $\ominus\oplus$: the separated valence state to the schematic unit; δ^- : the shared valence state to the schematic unit.

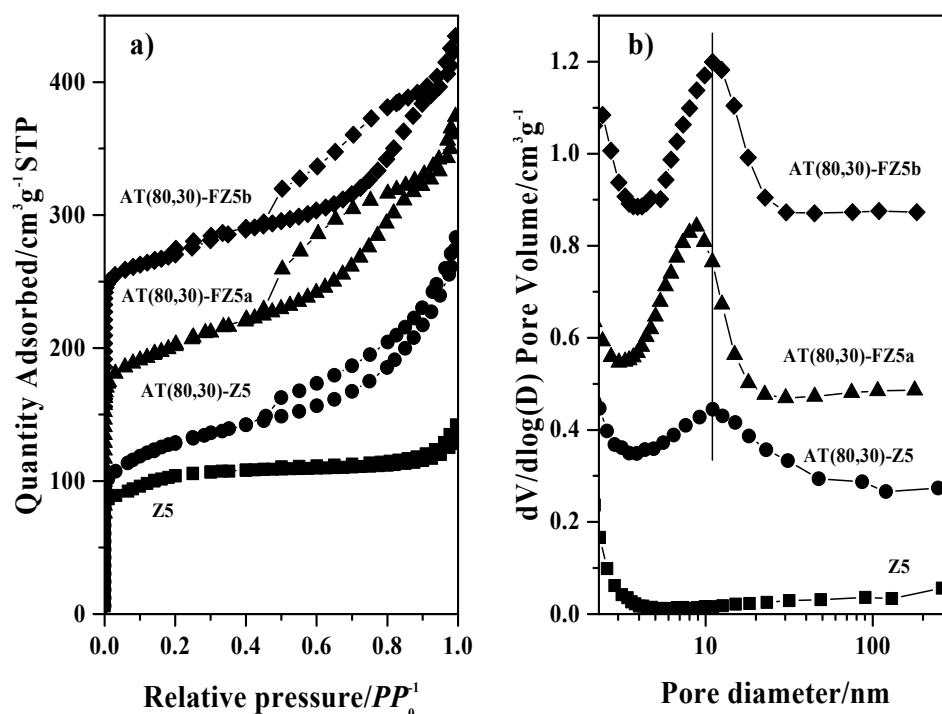


Figure 8. (a) N_2 adsorption-desorption isotherms of sequential fluorination-alkaline treated samples. The alkaline treatment temperature is 80°C . (b) BJH pore size distribution derived from the adsorption branches of the isotherms. The isotherms for AT(80,30)-FZ5a and AT(80,30)-FZ5b were offset vertically by 70 and $150 \text{ cm}^3 \text{g}^{-1}$, respectively. (b) Barrett-Joyner-Halenda (BJH) pore size distribution (PSD) data derived from the adsorption branches of the isotherms. The PSD curves of AT(80,30)-Z5, AT(80,30)-FZ5a and AT(80,30)-FZ5b were offset vertically by 0.2 , 0.4 and $0.8 \text{ cm}^3 \text{g}^{-1}$, respectively.

3. Experimental Section

3.1. Sample Preparation

Sequential fluorination-desilication: The commercial ZSM-5 zeolite (Z5, Si/Al_{nominal} = 34, HuangMa Chemical Co., Ltd., Nanjing, China) was used as the starting material. The pristine ZSM-5 was firstly impregnated with the aqueous NH₄F solution according to the impregnation method. Typically, ZSM-5 powder was stirred in the NH₄F solution (0.32 M and 0.60 M, weight/volume ratio for zeolite to solution is 1:3) at room temperature for 8 h. The impregnated samples were dried at 120 °C overnight, and calcined at 550 °C for 3 h. The obtained sample is coded as FZ5a and FZ5b in which *a* (0.12 wt%) and *b* (0.23 wt%) corresponds to the F loading on Z5, respectively. Then, the fluorinated sample was then alkaline treated in a polypropylene flask by an aqueous NaOH solution (0.2 M) at 65 °C or 80 °C for 30 min or 60 min. The alkaline-treated samples were collected by centrifugation (4000 rpm for 5 min), thoroughly washed and dried at 120 °C overnight. Finally, these samples were transformed to protonic-form by a threefold ammonium-exchange (NH₄NO₃ solutions, 0.8 M) and subsequent calcination at 550 °C for 3 h. The final H-form zeolites are designated as AT(*x*, *y*)-FZ5a and AT(*x*, *y*)-FZ5b, where *x* and *y* represent the alkaline treatment temperature (°C) and alkaline treatment time (minutes), respectively.

Comparative spontaneous alkaline treatment: The spontaneous alkaline treatment of the same pristine ZSM-5 zeolite was conducted as the same procedures as described for the alkaline treatment of fluorinated zeolites. After the same ammonia-exchange and calcination steps, the obtained zeolite is designated as AT(*x*, *y*)-Z5, where *x* and *y* represent the alkaline treatment temperature (°C) and alkaline treatment time (minutes), respectively.

Comparative steaming-alkaline treatment: Pristine ZSM-5 zeolite powder was firstly pressed into pellets under 3.0 MPa for 1 min, and then crushed into granules of around 5 mm to minimize the pressure-drop during the steaming process. Approximately 10 g of zeolite granules were loaded in a fixed quartz reactor and heated to 600 °C with a ramp rate of 5.6 °C min⁻¹ in dry air flow under ambient pressure. Afterwards, water vapor (0.8 mL min⁻¹) was charged and the dry air flow was stopped. After 3 h of steaming treatment, the water injection was stopped, and the steamed zeolite was cooled and dried under air flow. The obtained zeolites are denoted as ST-Z5. These steamed samples were subsequently subjected to the same alkaline treatment as the above same procedures. After the same ammonia-exchange and calcination steps, the obtained zeolite is designated as AT(60, *y*)-ST-Z5, where *y* represents the alkaline duration in minutes.

3.2. Characterization

Nitrogen adsorption measurements were carried out at −196 °C on a Micromeritics ASAP-2020 analyzer. Prior to analysis, each sample was evacuated at 350 °C for 10 h. Field emission scanning electron microscope (FESEM) measurement was performed with JEOL JSM-7800F at an accelerating voltage of 5 kV. High resolution transmission electron microscopy (HRTEM) measurement was performed with a JEOL JEM-2100 at an accelerating voltage of 120 KV. Solid NMR spectra were recorded on Bruker AVANCE III 500 MHz spectrometer equipped with a 4 mm MAS probe. ²⁷Al MAS NMR spectra were recorded at a resonance frequency of 130.3 MHz with a spinning rate of 12 KHz. Chemical shifts were referenced to 1 M of Al(NO₃)₃ at 0 ppm as a reference. The spectra were accumulated for 1000 scans with $\pi/12$ flip angle and a 2 s pulse delay.

4. Conclusions

The sequential fluorination-alkaline treatment is committed to the tailoring of the siliceous ZSM-5 zeolite (Si/Al = 34). The spontaneous growth of mesoporosity inside siliceous ZSM-5 zeolite is thereby intervened by the antecedent fluorination step. As a consequence, the essential duration for the achievement of well-defined mesoporosity is extended from 30 min for pristine zeolite to 60 min for the fluorinated zeolite. The fluorination leads to the various alterations to the framework sites as the function of fluorination level: perturbation of the environment of framework Al sites due to the Al-

F complexation, dealumination to the octa-coordinated non-framework Al species and formation of octa-coordinated aluminum fluoride phases. At least, the introduction of fluorine-ligand gives simultaneous electronic and steric impacts on the interplay between fluorinated zeolite and alkaline medium. Upon the low fluorination level, the charge effect overtakes that steric effect, which intensifies the electronic repulsion to the alkaline medium and therefore decelerates the mesoporosity growth. On the other hand, the steric effect overtakes the charge effect at the high fluorination level for F-coordinated non-framework Al species and eases the strong repulsion to the hydroxides. Compared to the inhibitive effect imposed by steaming, high level fluorination brings an enabling effect for mesoporosity growth. The impacts of fluorination-alkaline treatment on the mesoporosity growth of siliceous zeolite uncover more sides of the interplay between framework/non-framework Al species and alkaline medium, and provide insights into the understanding of the tailoring of porosities.

Author Contributions: Conceptualization, G.L., J.Z. and S.H.; Methodology, Z.G., M.H. and D.Z.; Experiments, Z.G., M.H., Y.Y., H.G. and K.Y.; Project administration, G.L. and J.Z.; Writing—original draft preparation, Z.G., M.H. and Y.Y.; Writing—review and editing, Z.G., Y.Y., K.Y. and S.H.; Supervision and funding acquisition, S.H. All authors have read and agreed to the published version of the manuscript.

Funding: Dalian Bureau of Science and Technology (No. 2020JJ25CY007) and National Natural Science Foundation of China (No. 21978282).

Data Availability Statement: All the data generated or analyzed within the present investigation are included in this manuscript.

Acknowledgments: This work was supported by CenerTech Tianjin Chemical Research and Design Institute (Co., Ltd.), Dalian Bureau of Science and Technology (No. 2020JJ25CY007) and National Natural Science Foundation of China (No. 21978282).

Conflicts of Interest: The authors declare no conflict of interest in publishing the results.

References

1. Vermeiren, W.; Gilson, J.-P. Impact of Zeolites on the Petroleum and Petrochemical Industry. *Top. Catal.* **2009**, *52*, 1131–1161. [[CrossRef](#)]
2. Primo, A.; Garcia, H. Zeolites as catalysts in oil refining. *Chem. Soc. Rev.* **2014**, *43*, 7548–7561. [[CrossRef](#)] [[PubMed](#)]
3. Choudary, N.V.; Newalkar, B.L. Use of zeolites in petroleum refining and petrochemical processes: Recent advances. *J. Porous Mater.* **2011**, *18*, 685–692. [[CrossRef](#)]
4. Dai, W.J.; Zhang, L.N.; Liu, R.Z.; Wu, G.J.; Guan, N.J.; Li, L.D. Plate-Like ZSM-5 Zeolites as Robust Catalysts for the Cracking of Hydrocarbons. *ACS Appl. Mater. Interfaces* **2022**, *14*, 11415–11424. [[CrossRef](#)] [[PubMed](#)]
5. Jacobs, P.A.; Dusselier, M.; Sels, B.F. Will Zeolite-Based Catalysis be as Relevant in Future Biorefineries as in Crude Oil Refineries? *Angew. Chem. Int. Ed.* **2014**, *53*, 8621–8626. [[CrossRef](#)]
6. Davis, M.E. Ordered porous materials for emerging applications. *Nature* **2002**, *417*, 813–821. [[CrossRef](#)]
7. Perego, C.; Millini, R. Porous materials in catalysis: Challenges for mesoporous materials. *Chem. Soc. Rev.* **2013**, *42*, 3956–3976. [[CrossRef](#)]
8. Nuttens, N.; Verboekend, D.; Deneyer, A.; Van Aelst, J.; Sels, B.F. Potential of Sustainable Hierarchical Zeolites in the Valorization of α -Pinene. *Chemsuschem* **2015**, *8*, 1197–1205. [[CrossRef](#)]
9. Dapsens, P.Y.; Mondelli, C.; Pérez-Ramírez, J. Biobased Chemicals from Conception toward Industrial Reality: Lessons Learned and To Be Learned. *ACS Catal.* **2012**, *2*, 1487–1499. [[CrossRef](#)]
10. Smith, K.; El-Hiti, G.A. Use of zeolites for greener and more *para*-selective electrophilic aromatic substitution reactions. *Green Chem.* **2011**, *13*, 1579–1608. [[CrossRef](#)]
11. Liu, Y.; Zhang, Q.; Li, J.; Wang, X.; Terasaki, O.; Xu, J.; Yu, J. Protozeolite-Seeded Synthesis of Single-Crystalline Hierarchical Zeolites with Facet-Shaped Mesopores and Their Catalytic Application in Methanol-to-Propylene Conversion. *Angew. Chem. Int. Ed.* **2022**, *134*, e202205716. [[CrossRef](#)]
12. Mardiana, S.; Azhari, N.J.; Ilmi, T.; Kadja, G.T.M. Hierarchical zeolite for biomass conversion to biofuel: A review. *Fuel* **2022**, *309*, 122119. [[CrossRef](#)]
13. Verboekend, D.; Pérez-Ramírez, J. Design of hierarchical zeolite catalysts by desilication. *Catal. Sci. Technol.* **2011**, *1*, 879–890. [[CrossRef](#)]

14. Pérez-Ramírez, J.; Mitchell, S.; Verboekend, D.; Milina, M.; Michels, N.-L.; Krumeich, F.; Marti, N.; Erdmann, M. Expanding the Horizons of Hierarchical Zeolites: Beyond Laboratory Curiosity towards Industrial Realization. *ChemCatChem* **2011**, *3*, 1731–1734. [[CrossRef](#)]
15. Kerstens, D.; Smeyers, B.; Waeyenberg, J.V.; Zhang, Q.; Yu, J.; Sels, B.F. State of the Art and Perspectives of Hierarchical Zeolites: Practical Overview of Synthesis Methods and Use in Catalysis. *Adv. Mater.* **2020**, *32*, 2004690. [[CrossRef](#)]
16. Fernandez, S.; Ostraat, M.L.; Zhang, K. Toward rational design of hierarchical beta zeolites: An overview and beyond. *AIChE J.* **2020**, *66*, e16943. [[CrossRef](#)]
17. Wang, Z.; Zhang, R.; Wang, J.; Yu, Z.; Xiang, Y.; Kong, L.; Liu, H.; Ma, A. Hierarchical zeolites obtained by alkaline treatment for enhanced n-pentane catalytic cracking. *Fuel* **2022**, *313*, 122669. [[CrossRef](#)]
18. Abdulridha, S.; Zhang, R.; Xu, S.; Tedstone, A.; Ou, X.; Gong, J.; Mao, B.; Frogley, M.; Bawn, C.; Zhou, Z.; et al. An efficient microwave-assisted chelation (MWAC) post-synthetic modification method to produce hierarchical Y zeolites. *Microporous Mesoporous Mater.* **2021**, *311*, 110715. [[CrossRef](#)]
19. Ogura, M.; Shinomiya, S.-Y.; Tateno, J.; Nara, Y.; Nomura, M.; Kikuchi, E.; Matsukata, M. Alkali-treatment technique—New method for modification of structural and acid-catalytic properties of ZSM-5 zeolites. *Appl. Catal. A Gen.* **2001**, *219*, 33–43. [[CrossRef](#)]
20. Groen, J.C.; Peffer, L.A.A.; Moulijn, J.A.; Pérez-Ramírez, J. Mechanism of Hierarchical Porosity Development in MFI Zeolites by Desilication: The Role of Aluminium as a Pore-Directing Agent. *Chem. Eur. J.* **2005**, *11*, 4983–4994. [[CrossRef](#)]
21. de Jong, K.P.; Zecevic, J.; Friedrich, H.; de Jongh, P.E.; Bulut, M.; van Donk, S.; Kenmogne, R.; Finiels, A.; Hulea, V.; Fajula, F. Zeolite Y Crystals with Trimodal Porosity as Ideal Hydrocracking Catalysts. *Angew. Chem. Int. Ed.* **2010**, *49*, 10074–10078. [[CrossRef](#)] [[PubMed](#)]
22. van Laak, A.N.C.; Sagala, S.L.; Zecevic, J.; Friedrich, H.; de Jongh, P.E.; de Jong, K.P. Mesoporous mordenites obtained by sequential acid and alkaline treatments—Catalysts for cumene production with enhanced accessibility. *J. Catal.* **2010**, *276*, 170–180. [[CrossRef](#)]
23. Huang, S.; Liu, X.; Yu, L.; Miao, S.; Liu, Z.; Zhang, S.; Xie, S.; Xu, L. Preparation of hierarchical mordenite zeolites by sequential steaming-acid leaching-alkaline treatment. *Microporous Mesoporous Mater.* **2014**, *191*, 18–26. [[CrossRef](#)]
24. Sammoury, H.; Toufaily, J.; Cherry, K.; Hamieh, T.; Pouilloux, Y.; Pinard, L. Impact of desilication of * BEA zeolites on the catalytic performance in hydroisomerization of n-C₁₀. *Appl. Catal. A Gen.* **2018**, *551*, 1–12. [[CrossRef](#)]
25. van Laak, A.N.C.; Zhang, L.; Parvulescu, A.N.; Bruijninx, P.C.A.; Weckhuysen, B.M.; de Jong, K.P.; de Jongh, P.E. Alkaline treatment of template containing zeolites: Introducing mesoporosity while preserving acidity. *Catal. Today* **2011**, *168*, 48–56. [[CrossRef](#)]
26. Zhang, D.; Jin, C.; Zou, M.; Huang, S. Mesopore Engineering for Well-Defined Mesoporosity in Al-Rich Aluminosilicate Zeolites. *Chem. Eur. J.* **2019**, *25*, 2675–2683. [[CrossRef](#)]
27. Groen, J.C.; Moulijn, J.A.; Pérez-Ramírez, J. Alkaline Posttreatment of MFI Zeolites. From Accelerated Screening to Scale-up. *Ind. Eng. Chem. Res.* **2007**, *46*, 4193–4201. [[CrossRef](#)]
28. Yu, L.; Xie, S.; Huang, S.; Xu, L. A Facile Top-Down Protocol for Postsynthesis Modification of Hierarchical Aluminum-Rich MFI Zeolites. *Chem. Eur. J.* **2015**, *21*, 1048–1054. [[CrossRef](#)]
29. Groen, J.C.; Moulijn, J.A.; Pérez-Ramírez, J. Decoupling mesoporosity formation and acidity modification in ZSM-5 zeolites by sequential desilication-dealumination. *Microporous Mesoporous Mater.* **2005**, *87*, 153–161. [[CrossRef](#)]
30. Silaghi, M.C.; Chizallet, C.; Raybaud, P. Challenges on molecular aspects of dealumination and desilication of zeolites. *Microporous Mesoporous Mater.* **2014**, *191*, 82–96. [[CrossRef](#)]
31. Yang, S.; Yu, C.; Yu, L.; Miao, S.; Zou, M.; Jin, C.; Zhang, D.; Xu, L.; Huang, S. Bridging Dealumination and Desilication for the Synthesis of Hierarchical MFI Zeolites. *Angew. Chem. Int. Ed.* **2017**, *56*, 12553–12556. [[CrossRef](#)] [[PubMed](#)]